Propagation properties of an optical vortex carried by an Airy beam: experimental implementation

H. T. Dai,[1] Y. J. Liu,[2] D. Luo,[2] and X. W. Sun[1,2,*]

[1]*Department of Applied Physics, School of Science, Tianjin University, Tianjin 300072, China*

[2]*School of Electrical and Electronic Engineering, Nanyang Technological University, Nanyang Avenue, Singapore 639798, Singapore*

**Corresponding author: exwsun@ntu.edu.sg*

Received January 3, 2011; revised March 25, 2011; accepted March 28, 2011; posted March 30, 2011 (Doc. ID 140362); published April 27, 2011

In this Letter, we experimentally studied the propagation dynamics of Airy beams (AiBs) carrying phase singularity or an optical vortex (OV). A $3/2$ phase mask encoded with phase singularity was used to generate AiBs and OVs enjoying precise position alignment and compact optical configuration simultaneously. Experimental results showed that the OV deflection velocity was faster than that of the main lobe of the AiB, agreeing with the analytical prediction. Numerical simulation results are also in agreement with the experimental results. Furthermore, OVs with larger topological charges were also studied experimentally with the same approach. © 2011 Optical Society of America

OCIS codes: 260.0260, 350.5500, 050.1940.

Recently, Airy beams (AiBs) have attracted intensive interest [1–9]. Though the concept of the Airy wave package could go back 30 years, its counterpart in optics was only demonstrated recently [2]. Thus far, Airy-type beams have been studied considerably, including generation methods [2,6], propagation dynamics [4], and potential applications [5,7,9]. Most recently, we have theoretically investigated the propagation dynamics of an optical vortex (OV) carried by AiBs [10] and showed that the OV will experience a transverse deflection as conventional AiBs do, but with a double deflected velocity before a critical position z_s, where the transverse deflection of the OV is equal to that of the main lobe of the AiB and yields an AiB's main lobe with donut profile. With further propagation, the distorted main lobe will be reconstructed gradually. At last, the phase singularity will appear again in the middle of the AiB after a long enough propagation distance. To generate this kind of compound beam in the experiment, an intuitive approach is to introduce OVs into AiBs by placing a spiral phase plate (SPP) at the Fourier plane of the cubic phase mask. Nevertheless, there is little freedom on the alignment to ensure a precise displacement between the center of the SPP and the main lobe of the AiB within the small effective area in the focal plane of the Fourier lens.

Very recently, Mazilu *et al.* [11] experimentally studied OV-embedded AiBs and successfully achieved accelerating vortices in AiBs [2] by employing a spiral phase on a cubic phase pattern. However, the overall propagation dynamics of OV-embedded AiBs could not be obtained [11] explicitly. Therefore, a generating method for AiBs containing an OV that displays compact optical configuration and precise alignment of the AiB and OV is required. For this, we first consider the generation method of OVs, which is realized by virtue of a hologram such as forklike gratings [12,13]. On the other hand, Cottrell *et al.* adopted a $3\pi/2$ phase mask to generate AiBs [14] with a compact optical setup. Combining these two methods, we can encode an OV into AiBs with the desired dislocation between the OV and AiB in a compact optical configuration. In this Letter, we will experimentally investigate the propagation dynamics of OVs carried by AiBs by encoding a phase singularity into a $3/2$ phase pattern, which is implemented by a phase spatial light modulator (pSLM).

According to the direct generation method described in [14], the AiBs can be generated by a $3/2$ phase profile as

$$\phi(x,y) = 8\pi a(x^{3/2} + y^{3/2})/(3\lambda), \tag{1}$$

where a is the parameter to determine the parabolic curve, and x, y are the transvers coordinate respectively.

Considering the combination of a phase singularity and $3/2$ phase profile, the phase pattern can be written as

$$\phi(x,y) = 8\pi a(x^{3/2} + y^{3/2})/(3\lambda) + l\arg[(x - x_d) + i(y - y_d)], \tag{2}$$

where arg[.] denotes the argument of the complex number, i is the imaginary unit, and x_d and y_d denote the dislocation between the center of phase singularity (CPS) and the center of the main lobe of the Airy beam (CAiB) along x and y axis directions, respectively. λ is the wavelength of incident light, and l represents the topological charge of the OV. The CPS is defined as the symmetric center of the phase singularity, whereas the origin ($x = 0$ and $y = 0$) of the coordinate is set as the CAiB. In our configuration, the CAiB locates at the bottom left corner of the phase mask, as shown in Fig. 1. The forking shapes pointed by the red arrows in Figs. 1(a) and 1(b) are due to the superimposition of the spiral phase and $3/2$ phase pattern.

In our experiments, linearly polarized light from a He–Ne laser with a wavelength of 633 nm was impinged onto the surface of a pSLM (HoloEye model LCR2500, pixels: 1024×768, pixel spacing: $19\,\mu$m). The linear phase

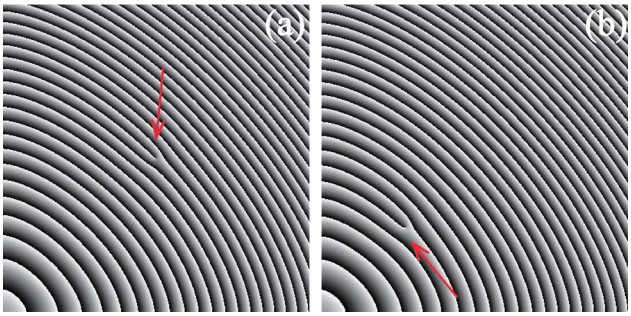

Fig. 1. (Color online) Phase patterns encoded onto a pSLM for generating AiBs with an OV; the parameters are set as $a = 0.00155\,\mathrm{mm}^{-0.5}$, $l = 1$, and (a) $x_d = y_d = 3.8\,\mathrm{mm}$, (b) $x_d = y_d = 2.09\,\mathrm{mm}$.

modulation was achieved by combination of a linear polarizer and suitable internal gamma correction for the device. We recorded the intensity profiles at different propagation distances from the pSLM using a CCD camera (DataRay WinCamD, pixel spacing: $13.4\,\mu$m). Figures 1(a) and 1(b) show the phase profile exerted on the pSLM for simultaneous AiB and OV generation with various dislocations. The figures were rescaled for clarity. It is worth mentioning that gray scale mapped phase values (0 and 255 for zero and 2π phase modulation, respectively) have been wrapped in the range from 0 to 2π.

The intensity distributions of the AiBs carrying an OV with a unit topological charge at different propagation distances with various beam parameters are then investigated experimentally. Figures 2(a)–2(d) show snapshots of intensity profiles of the AiBs with an OV located at four different propagation distances. The experimental parameters used are $a = 0.00155\,\mathrm{mm}^{-0.5}$, $x_d = y_d = 2.09\,\mathrm{mm}$, $z = \{30, 50, 80, 110\}$ cm. Figures 2(e)–2(h) show the intensity profiles in Figs. 2(a)–2(d) with the same a and z, but different x_d and y_d ($x_d = y_d = 3.8\,\mathrm{mm}$). Figures 2(i)–2(l) show the same intensity distributions as those in Figs. 2(a)–2(d) with a different a ($a = 0.00165\,\mathrm{mm}^{-0.5}$) value, and Figs. 2(m)–2(p) show the same intensity profiles as Figs. 2(i)–2(l), but with different x_d and y_d ($x_d = y_d = 3.8\,\mathrm{mm}$) values. To show the fine structures of the intensity profiles, all the images shown in Fig. 2 are in logarithmic scale. According to the experimental results, it is clear that the transverse deflection velocity of an OV is larger than that of the main lobe of a conventional AiB. Though the initial position of the OV is behind the main lobe, it can catch up with the main lobe of the AiB at a certain distance, which results in a distorted main lobe as shown in Figs. 2(c), 2(g), 2(l), and 2(p). The inset of Fig. 2(c) depicts the magnified image of the distorted main lobe. With further propagating, the OV, however, cannot exceed the main lobe due to the intrinsic property of Airy function (the values of Airy function will decrease exponentially as the coordinate is larger than that of main lobe). It will reform in the middle of the AiB's intensity profile as in the inset of Fig. 2(d), which was recorded by CCD far away from the pSLM. So far, the main lobe will be reconstructed when the AiB propagates further, due to its self-healing property. The ghost images in the first column in Fig. 2 are due to higher diffractive orders [14].

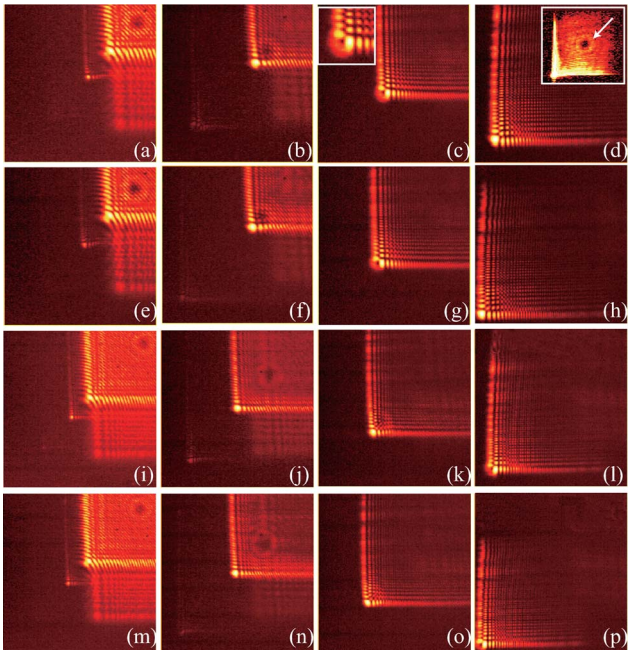

Fig. 2. (Color online) Experimental snapshots of intensity profiles of AiBs with an OV embedded for various parameters of $a = \{0.00155, 0.00165, 0.00155, 0.00165\}\,\mathrm{mm}^{-0.5}$ (rows) corresponding to various dislocations of $x_d = y_d = \{2.09, 2.09, 3.8, 3.8\}$ mm located at distances (columns) of $z = \{30, 50, 80, 110\}$ cm.

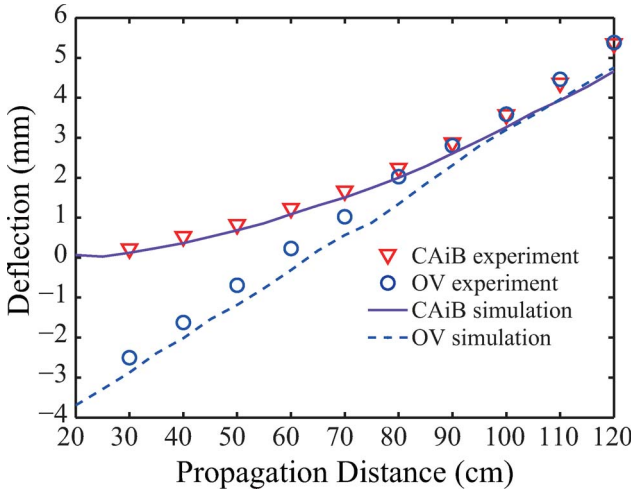

Fig. 3. (Color online) Numerically simulated and experimental trajectories of a CAiB and an OV. The beam parameters are set as $x_0 = 0.098\,\mathrm{mm}$ and $x_d = y_d = 3.08\,\mathrm{mm}$.

To manifest the behavior of the OV and CAiB more clearly, we present the trajectories of the OV and CAiB

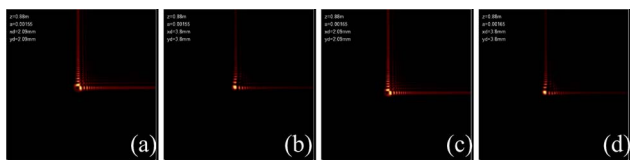

Fig. 4. (Color online) Numerically simulated results of propagation dynamics of OVs embedded in AiBs with various parameters: (a) $a = 0.00155\,\mathrm{mm}^{-0.5}$, $x_d = y_d = 2.09\,\mathrm{mm}$ (Media 1), (b) $a = 0.00155\,\mathrm{mm}^{-0.5}$, $x_d = y_d = 3.8\,\mathrm{mm}$ (Media 2), (c) $a = 0.00165\,\mathrm{mm}^{-0.5}$, $x_d = y_d = 2.09\,\mathrm{mm}$ (Media 3), (d) $a = 0.00165\,\mathrm{mm}^{-0.5}$, $x_d = y_d = 3.8\,\mathrm{mm}$ (Media 4).

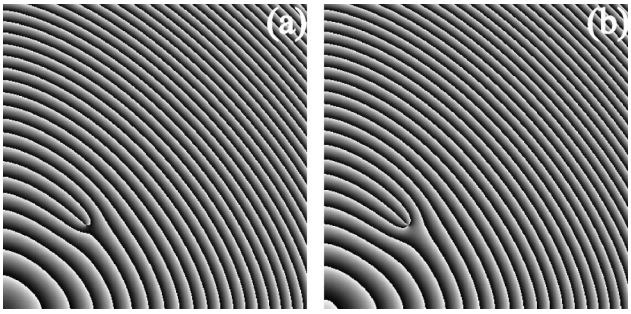

Fig. 5. Phase patterns for generating AiBs with higher order OVs; the parameters are set as $a = 0.00155\,\mathrm{mm}^{-0.5}$, $x_d = y_d = 2.09\,\mathrm{mm}$, and (a) $l = 2$, (b) $l = 3$.

in Fig. 3 simultaneously. The beam parameters used here are $a = 0.00165\,\mathrm{mm}^{-0.5}$, $x_d = y_d = 3.08\,\mathrm{mm}$ and $x_0 = (1/4a^2k^2)^{1/3} = 0.098\,\mathrm{mm}$, where $k = 2\pi/\lambda$ and λ is the wavelength of the incident light. It can be seen that the experiment matches with the simulation well for both the OV and CAiB, whereas the OV walks along a straight line rather than a parabola as theoretically predicated [10]. The phenomenon can be understood as follows. When the OV is far away from the CAiB initially, the 3/2 phase profile [Eq. (1)] is relatively even and can be regarded as a linear phase background. When the OV is getting close to the CAiB, its trajectory becomes parabolic.

Figures 4(a)–4(d) show the simulated dynamics propagation of the unit-charged OV embedded in an AiB, which is coincident with the experimental results.

We also investigated the effect of OVs with larger topological charges on the propagation dynamics of AiBs. Figures 5(a) and 5(b) depict the combined phase patterns of the OVs with topological charges of 2 and 3 embedded in a 3/2 phase pattern, respectively. The corresponding experimental results are shown in Figs. 6(a)–6(h). It is interesting to note that topological charge number has no obvious effect on the transverse deflection velocity of an OV, which is due to the unchanged background optical field [15], whereas the distorted main lobes, as depicted in Figs. 6(c) and 6(g), lose the symmetric "donut" profile, which is caused by the nonsymmetric field of the carrier wave, i.e., the AiB. Similar to the charge 1 OV beam case, the revival of the multiple-charged OV in the middle of the AiB was observed experimentally after a long propagation distance. The intensity profiles in Fig. 4 are also drawn in log scale for a better visibility. According to the experimental results, the combined beam of an OV and AiB will propagate regardless of the topological charges of the OV. Further numerical simulations confirmed this result.

In conclusion, we have experimentally demonstrated the propagation dynamics of OVs carried by AiBs using a 3/2 phase mask encoded on a pSLM. This method overcomes the difficulty of aligning the center of both AiBs and OVs with compact optical configurations, providing a practical way to generate OV-embedded AiBs for

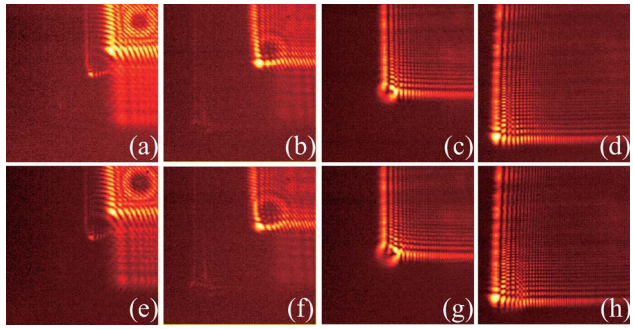

Fig. 6. (Color online) Experimental intensity profiles of AiBs with higher order OVs at different propagation distances (a) and (e) $z = 30\,\mathrm{cm}$, (b) and (f) $z = 50\,\mathrm{cm}$, (c) and (g) $z = 80\,\mathrm{cm}$, (d) and (h) $z = 110\,\mathrm{cm}$ for topological charge 2 and 3, respectively.

further applications, such as particle clearing, multiple-plane trapping, etc. Experimental results proved the larger deflected velocity of the OV during propagation, which was predicted by theory. Further studies also showed that the larger topological charge of the OV (>1) would have no obvious effect on the propagation dynamics of an AiB with an OV embedded. Numerical simulated results are in good agreement with the experimental results.

This work was partially supported by the National Natural Science Foundation of China (NSFC) under Grant No. 61076015 and No. 61006037.

References

1. G. A. Siviloglou and D. N. Christodoulides, Opt. Lett. **32**, 979 (2007).
2. G. A. Siviloglou, J. Broky, A. Dogariu, and D. N. Christodoulides, Phys. Rev. Lett. **99**, 213901 (2007).
3. I. M. Besieris and A. M. Shaarawi, Opt. Lett. **32**, 2447 (2007).
4. G. A. Siviloglou, J. Broky, A. Dogariu, and D. N. Christodoulides, Opt. Lett. **33**, 207 (2008).
5. A. Chong, W. H. Reninger, D. N. Christodoulides, and F. W. Wise, Nat. Photon. **4**, 103 (2010).
6. T. Ellenbogen, N. Voloch-Bloch, A. Ganany-Padowicz, and A. Arie, Nat. Photon. **3**, 395 (2009).
7. P. Polynkin, M. Kolesik, J. V. Moloney, G. A. Siviloglou, and D. N. Christodoulides, Science **324**, 229 (2009).
8. H. T. Dai, X. W. Sun, D. Luo, and Y. J. Liu, Opt. Express **17**, 19365 (2009).
9. Y. L. Gu and G. Gbur, Opt. Lett. **35**, 3456 (2010).
10. H. T. Dai, Y. J. Liu, D. Luo, and X. W. Sun, Opt. Lett. **35**, 4075 (2010).
11. M. Mazilu, J. Baumgartl, T. Cizmar, and K. Dholakia, Proc. SPIE **7430**, 74300C (2009).
12. Y. J. Liu, X. W. Sun, Q. Wang, and D. Luo, Opt. Express **15**, 16645 (2007).
13. Y. J. Liu, X. W. Sun, D. Luo, and Z. Raszewski, Appl. Phys. Lett. **92**, 101114 (2008).
14. D. M. Cottrell, J. A. Davis, and T. M. Hazard, Opt. Lett. **34**, 2634 (2009).
15. D. Rozas, C. T. Law, and G. A. Swartzlander, J. Opt. Soc. Am. B **14**, 3054 (1997).